Werk

Jahr: 1974
Kollektion: fid.geo
Signatur: 8 Z NAT 2148:40
Digitalisiert: Niedersächsische Staats- und Universitätsbibliothek Göttingen
Werk Id: PPN1015067948_0040
PURL: http://resolver.sub.uni-goettingen.de/purl?PPN1015067948_0040

LOG Id: LOG_0053
LOG Titel: On a high-frequency method for the measurement of susceptibilities and hysteresis losses of rocks and minerals between nitrogen temperature and 700 °C
LOG Typ: article

Übergeordnetes Werk

Werk Id: PPN1015067948
PURL: http://resolver.sub.uni-goettingen.de/purl?PPN1015067948
OPAC: http://opac.sub.uni-goettingen.de/DB=1/PPN?PPN=1015067948

Contact

Niedersächsische Staats- und Universitätsbibliothek Göttingen
Georg-August-Universität Göttingen
Platz der Göttinger Sieben 1
37073 Göttingen
Germany
Email: gdz@sub.uni-goettingen.de

J. Geophys. 40, 303–328, 1974

On a High-Frequency Method for the Measurement of Susceptibilities and Hysteresis Losses of Rocks and Minerals between Nitrogen Temperature and 700 °C

H. Markert
Gesamthochschule Bamberg

K.-H. Trissl, G. J. Zimmermann
Sektion Physik, Universität München

Received August 31, 1973; Revised Version December 17, 1973

Abstract. A high-frequency method is described that, working at 10 megacycles, enables very sensitive measurements of magnetic, paramagnetic and even diamagnetic susceptibilities and losses of rocks and minerals within a temperature interval ranging from —196 °C up to about 700 °C. The physical principle is explained and a detailed wiring scheme illustrates the technical realization. The evaluation of the output signal is based on a theory of measurement which yields three different measuring techniques, the advantages and disadvantages of which are also discussed. To succeed in getting absolute results a somewhat sophisticated calibration procedure is worked out and has been tested using salts of known paramagnetic properties. Some experimental results finally exemplify the wide ranges of sensitivity and applicability of the method.

Key words: Magnetic Susceptibility — Hysteresis Loss — Magnetic Anisotropy — Curie Point — Phase Transition.

§ 1. Introduction

On the occasion of the 'NATO-conference on Paleomagnetic Methods', held in the Physics Department of the University of Newcastle upon Tyne, April 1—10, 1964, two different high-frequency methods have already been discussed with respect to their applicability to rock magnetism.

The first one, working on the priciple of a usual ac-inductivity bridge at a frequency of 1000 cycles/sec, has been described by Fuller (1967) who pointed at the relatively high sensitivity of such a technique and demonstrated its usefulness for anisotropy measurements. The second one, the so-called Fraunberger high-frequency method, see Fraunberger (1955), was explained by Petersen (1967). It is working at 10 megacycles/sec on the principle of two coupled oscillating circuits one of which contains the

sample as a core of its oscillating coil. This latter method, measuring mainly the high-frequency losses, was emphasized to be quite helpful in determining Curie points of rocks.

Reading these papers, one easily gets the impression that both methods represent two opposite limiting cases of one ideal measuring principle which however might be synthetized from them and which then should be suitable for performing very sensitive simultaneous measurements of susceptibilities and losses as well. In fact, according to Ehrenfest (1933) high-frequency losses are extremely sensitive to transitions of Curie points and generally to all kinds of second order phase transitions which cause sharp maxima of such losses. On the other hand the susceptibility's tensor character is a sufficient basis for anisotropy measurements.

The aim of the present work was therefore to combine both earlier methods in order to develop at least an approximation to that 'ideal' measuring principle. When we had to decide whether to start from Fuller's bridge or from Fraunberger's high-frequency method we preferred the latter because of its use of oscillating circuits which we regarded to be a necessary condition for achieving high sensitivity. A more detailed experimental study of the original Fraunberger apparatus however brought some imperfections to light which turned out to be rather unfavourable and should thus be avoided when developing the new device:

1. to get the measuring results, the system of coupled oscillating circuits so far had to be retuned at each measuring point, i.e. for instance after each variation of the temperature or any other parameter; thus no automatic recording could be carried out at all;

2. as no detailed theory of the real measuring device ever had been worked out mathematically, it remained somewhat mysterious how the susceptibility could have been measured at all;

3. it was completely unclear how to use that apparatus for simultaneous measurements of susceptibilities and losses;

4. one of the most important fields of application, the determination of the spectrum of Curie points of a given rock, was limited to rather volumenous and strong magnetic samples only because of the difficulty to avoid a very marked increase of the zero signal with increasing temperature caused by the temperature-dependent losses of the coil and of the furnace material itself; additionally that undesirable effect showed a considerable temperature hysteresis as is illustrated in Fig. 1 by the dashed curves.

We think however that we could succeed in overcoming these difficulties and it is another purpose of the following sections to report on our solutions of the above sketched problems.

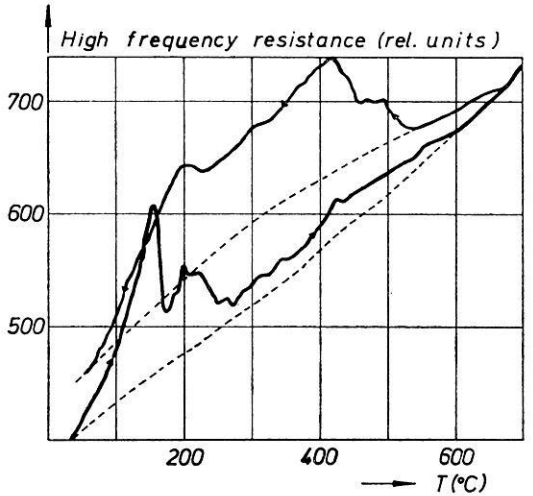

Fig. 1. Measuring example shown by Petersen (1967) in order to illustrate the applicability of the original Fraunberger high-frequency method. The output signal, being proportional to the high-frequency losses, was obtained during a heat treatment of a basalt sample of the 'Rauher Kulm'. For comparison with our respective results see Fig. 7 and § 4., point 2. The dashed curves are due to temperature hysteresis caused by temperature-dependent losses of the measuring coil, the sample container and the furnace material

§ 2. The Modified High-Frequency Apparatus

The original 'Fraunberger apparatus' was first described by Fraunberger (1955) and by Schwarz (1963). Its idealized wiring diagram, sketched in Fig. 2, shows the apparatus which consists mainly of a quartz-stabilized high-frequency generator working at about 10 megacycles per second and driving two inductively coupled oscillating circuits each of which again is coupled to a respective recording device consisting of a rectifier diode followed by a low band pass connected in series with a galvanometer.

The disadvantages of such a rather simple device are obvious:

a) no automatic recording;

b) no sufficiently clear separation between the high-frequency generator and the oscillating circuits;

c) low signal/noise ratio at the outputs of the registrating devices;

d) no zero suppress.

Thus, in order to realize the improvements announced in § 1, we modified the wiring scheme of Fig. 2 into that one shown in Fig. 3. As may be seen from that figure, the new device just eliminates the weak points summarized above, i.e. the new apparatus is working with:

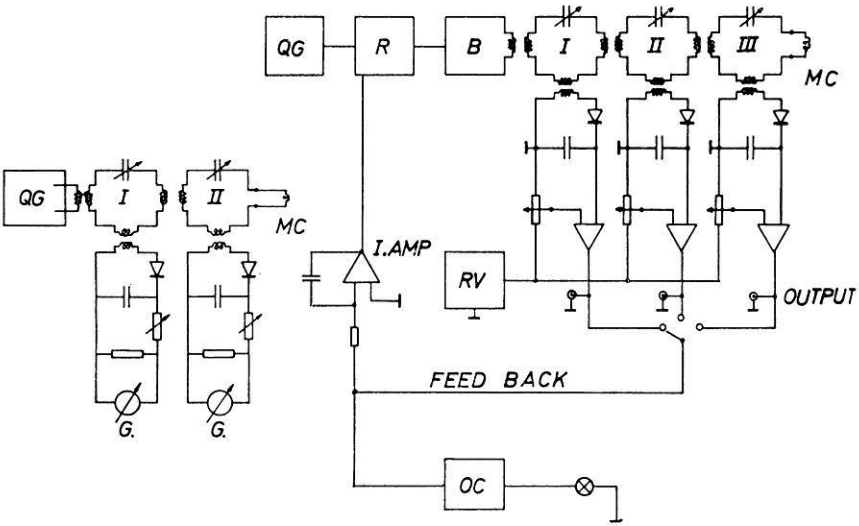

Fig. 2

Fig. 3

Fig. 2. Wiring scheme of the original Fraunberger high-frequency apparatus, see Fraunberger (1955). *QG.*: quartz generator, *MC*: measuring coil, *G*: galvanometer

Fig. 3. Wiring scheme of the modified high-frequency apparatus. *QG* quartz generator, *R* regulating equipment, *B* buffer, *MC* measuring coil, *I.AMP* integrating amplifier, *RV* reference voltage, *OC* overrange control

1. three oscillating circuits the currents in each of wich alternatively can be kept extremely constant by means of an integrating feedback system (which trimms the amplitude of the regulated circuit to the amount indicated by the reference voltage of the respective recording device); particularly is it now possible to stabilize the amplitude in circuit I which then acts as an extremely constant, inductively coupled high-frequency generator;

2. much better signal/noise ratio for instance in circuits II and III if circuit I is stabilized;

3. a very wide-ranged zero suppress brought about by use of differential amplifiers in each recording device;

4. high output voltage up to ten volts;

5. an error device signalizing overload of the high-frequency generator.

As the clear separation between high-frequency generator and circuits II and III now allows exact theoretical treatment of the latter ones, it is sufficient now (according to the outline given in the succeeding § 3) to record the output signals as functions of the temperature (or of other ex-

ternal parameters) in order to evaluate the susceptibility as well as the high-frequency losses. Thus the condition of automatic recording also can be fulfilled — but besides, of course, it is still possible to use the former measuring technique proposed by Fraunberger (1955) and Petersen (1967).

Some brief remarks concerning the differential amplification of the measuring signal may be added:

a) the field-effect transistors at the input of each of the three low noise low bias current operational amplifiers have been carefully selected with respect to extremely low offset drift which was tested experimentally;

b) the reference voltage source is double-stabilized and gives a reference voltage of very low temperature coefficient; this voltage is calibrated over a range from 0.000 to 0.999 Volts and can be adjusted by a digital display;

c) each operational amplifier computes the difference between the rectified high-frequency voltage V_{HF} and the reference voltage $V_{Ref.}$, multiplicated by an amplification factor A, i.e.

$$V_{out} = A \cdot (V_{HF} - V_{Ref.}), \tag{1}$$

where

$$A = 1; 10; 100; 1000.$$

§ 3. Theory of the Measuring Procedure

I. General Concept

Starting in a similar way as Schwarz already had chosen in 1963 in order to develop a quantitative theory of the Fraunberger apparatus, we base our considerations on the following set of equations the physical meaning of which is also illustrated by the vector diagram shown in Fig. 4:

$$\tilde{U}_{12} + \tilde{U}_{32} = \tilde{I}_2 \cdot (R_2 + j \cdot \omega \cdot L_2 + 1/j \cdot \omega \cdot C_2) \tag{2}$$

$$\tilde{U}_{23} = \tilde{I}_3 \cdot (R_3 + j \cdot \omega \cdot L_3 + 1/j \cdot \omega \cdot C_3); \tag{3}$$

here the ac-voltage $\tilde{U}_{ik}$ induced in circuit k by means of inductive interaction with circuit i, is given by

$$\tilde{U}_{ik} = -j \cdot \omega \cdot L_{ik} \cdot \tilde{I}_i, \; i, k = 1; 2; 3; \tag{4}$$

with $j = (-1)^{1/2}$, with $L_{ik} = L_{ki}$ denoting the coupling inductance between circuits i and k, and with the ac-current $\tilde{I}_i$ of circuit i being represented by

$$\tilde{I}_i = I_i \cdot \exp(j \cdot (\omega \cdot t + \alpha_i)), \tag{5}$$

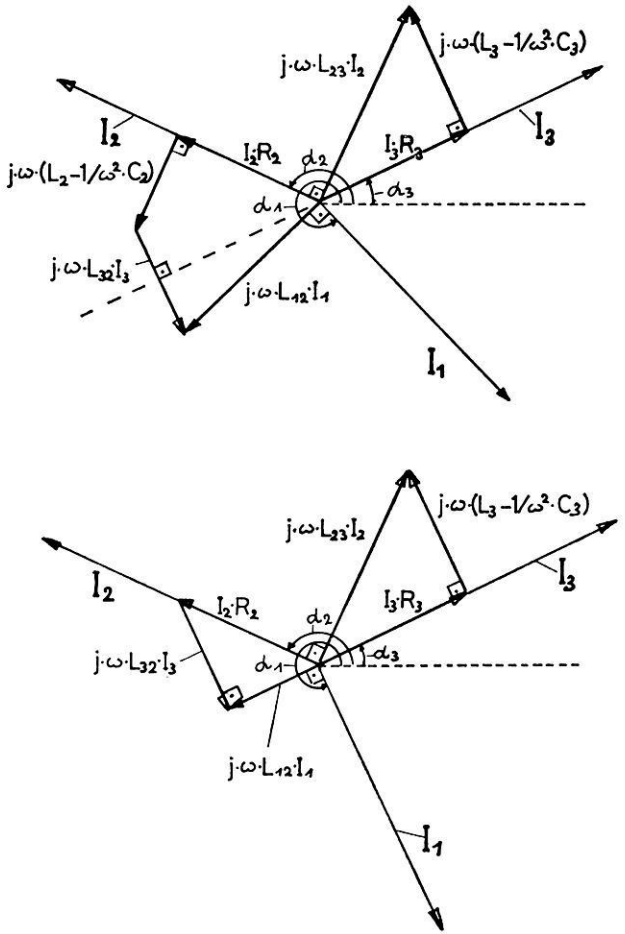

Fig. 4. Vector diagram illustrating the phase relations taking place in a system of three inductively coupled oscillating circuits. Fig. 4a. describes the more general case of $(L_2 - 1/\omega^2 \cdot C_2) > O$, while Fig. 4b. is true if circuit II is tuned to resonance, i.e. if $(L_2 - 1/\omega^2 \cdot C_2) = O$

where the α_i are defined in Fig. 4. The symbols R_2 and R_3, L_2 and L_3, and C_2 and C_3 designate the total resistance, the total inductance, and the variable capacity of circuits 2 and 3, respectively. Eqs. (2) and (3) hold true if there is no matter inside the coils or the condensors, i.e. if neither the magnetic nor the dielectric permeability differs from one. If however, particularly in circuit III, the magnetic permeability μ really differs from one — which is the case we have to discuss in the subsequent sections —, we can take into account this according to Feldtkeller (1949) and Kneller (1962), by adding

two sample-induced terms ΔL_3 and ΔR_3 to L_3 and R_3 of circuit III, respectively. Interpreted as functions of the real and imaginary part of the complex permeability

$$\bar{\mu} = \mu_r + j \cdot \mu_i, \tag{6}$$

according to Feldtkeller and Kneller, these terms can be written as

$$\Delta L_3 = \mu_r \cdot (n^2 \cdot F/l) \tag{7}$$

and

$$\Delta R_3 = \mu_i \cdot (\omega \cdot n^2 \cdot F/l), \tag{8}$$

where n means the number of windings of the measuring coil, F its cross section and l its length, respectively. In the case of $\bar{\mu} \neq 1$, Eq. (3) therefore has to be extended to the following expression

$$\tilde{U}_{23} = \tilde{I} \cdot (R_3 + \Delta R_3 + j \cdot \omega \cdot (L_3 + \Delta L_3) + 1/j \cdot \omega \cdot C_3) \tag{3a}$$

which — as well as the complemetnary Eq. (2) — will split into two equations if the respective terms $\tilde{U}_{ik}$, $\tilde{I}_k$ are substituted according to Eqs. (4) and (5), respectively. We then get the following system of basic equations:

$$R_3 + \Delta R_3 = \omega \cdot L_{23} \cdot (I_2/I_3) \cdot \cos \varphi \tag{9}$$

$$\omega \cdot (L_3 - 1/\omega^2 \cdot C_3) + \omega \cdot \Delta L_3 = \omega \cdot L_{23} \cdot (I_2/I_3) \cdot \sin \varphi \tag{10}$$

$$R_2 = \omega \cdot L_{12} \cdot (I_1/I_2) \cdot \cos \psi + \omega \cdot L_{32} \cdot (I_3/I_2) \cdot \cos \varphi \tag{11}$$

$$\omega \cdot L_2 - 1/\omega \cdot C_2 = \omega \cdot L_{12} \cdot (I_1/I_2) \cdot \sin \psi + \omega \cdot L_{32} \cdot (I_3/I_2) \cdot \sin \varphi, \tag{12}$$

where, according to Fig. 4a, the phase angles φ and ψ are given by

$$\varphi = (\alpha_2 - \alpha_3) - \pi/2 \tag{13}$$

and

$$\psi = (\alpha_1 - \alpha_2) - \pi/2. \tag{14}$$

The aim of the following considerations are relations of type

$$\Delta R_3/R_3 = f_1(\Delta I_3/I_3) \tag{15}$$

and

$$\omega \cdot \Delta L_3/R_3 = f_2(\Delta I_3/I_3), \tag{16}$$

with the symbol Δ meaning 'small deviation from . . .', and with the functions f_1 and f_2 being as simple as possible.

Trying thus to simplify Eqs. (9)—(12), we take advantage of all useful properties of the apparatus, namly:

a) the possibility of keeping alternatively constant either I_1 or I_2 or I_3;

b) the possibility of tuning all oscillating circuits independently of each other either to resonance or to special points of their resonance curves.

For instance if we tune circuits I and II to resonance and keep the amplitude I_2 of circuit II additionally constant, circuit II will work as a new and very constant high-frequency generator with respect to circuit III, i.e. we can completely forget the existence of circuit I and thus, in this case, we only have to deal with Eqs. (9) and (10) where however I_2 now is constant too.

Another possibility would be to regulate the amplitude I_3 of circuit III automatically constant and to measure simultaneously in circuit II which, as well as circuit I, should have been tuned to resonance before. Again, as in the case above, the evaluation of inductance and resistance has to start from Eqs. (9) and (10) only.

Finally we may keep constant the amplitude I_1 of circuit I which together with circuit II has been tuned to resonance before. In this case however it is necessary to measure I_2 and I_3 in circuits II and III *simultaneously*, and to use the total set Eqs. (9)—(12) in order to find out the sample-induced normalized changes $\Delta R_3/R_3$ and $\omega \cdot \Delta L_3/R_3$, respectively.

II. Quantitative Description of Three Measuring Procedures

1. Measurement of I_2 during Automatic Regulation of I_3

From a formal standpoint this technique seems to be the most elegant one. It starts from Eqs. (9) and (10) which can be simplified once more by introduction of an additional arbitrary condition, demanding that

$$(\omega \cdot L_3 - 1/\omega \cdot C_3^*)^2 = R_3^2 \tag{17}$$

— which can be fulfilled by two suitably chosen values $C_{3_1}^*$, $C_{3_2}^*$ — and meaning physically that circuit III without sample has to be tuned either to the high-capacity flank or to the low-capacity flank of its resonance curve the maximum of which has the coordinates $I_{3_{max}}$ and $C_{30} = 1/\omega^2 \cdot L_3$. To find the low-capacity value $C_3^l = C_{3_1}^*$ and the high-capacity solution $C_3^h = C_{3_2}^*$ experimentally, one only has to tune circuit III to resonance and then either to lower or to increase C_3 until I_3 has decreased from $I_{3_{max}}$ to $I_{3_{max}}/(2)^{1/2}$.

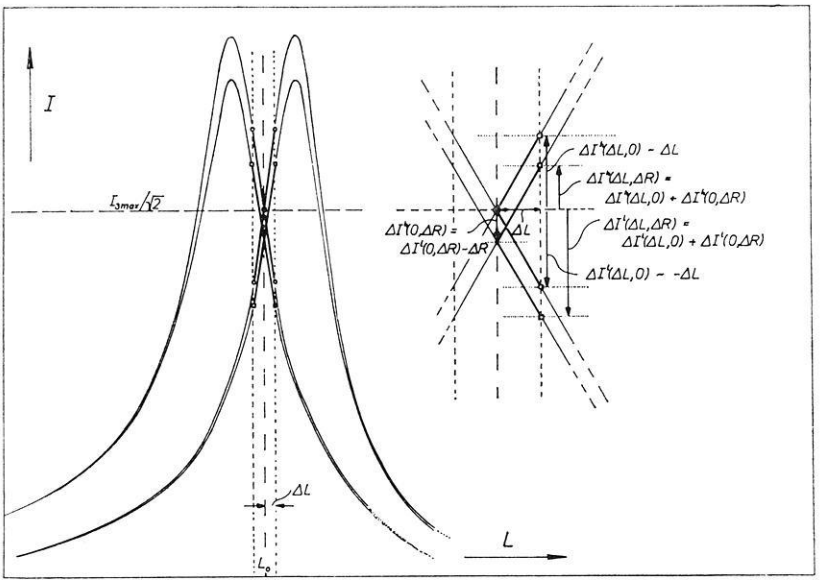

Fig. 5. Schematic representation of two pairs of resonance curves of circuit III shifted from the non-drawn original resonance curve (at $I_3 = I_{3_{max}}$ and $L_3 = L_{30} = 1/\omega^2 \cdot C_{30}$) to positions of higher ($L_{30} + \Delta L$) and lower ($L_{30} - \Delta L$) inductance, according to the instructions given by eq. (17) which defines the two corresponding capacity values C_3^l and C_3^h, respectively. If, in the case without sample, C_3 for instance is tuned to $C_3^l < C_{30}$, the current I_3, being proportional to $(R_3^2 + (\omega \cdot L_{30} - 1/\omega^2 \cdot C_3^l)^2)^{-1/2}$, will decrease to $I_{3_{max}}/\sqrt{2}$, and thus the system will be adjusted to its working point at the lower flank of the right-handed (undamped) resonance curve. Let now a sample be put into the measuring coil. Then an increase in inductance (ΔL) and an additional damping (ΔR) will occur, and the point of state of the oscillating system therefore has to move twice: once from (L_{30}; $I_{3_{max}}/\sqrt{2}$) to ($L_{30} + \Delta L$; $I_{3_{max}}/\sqrt{2} + \Delta I_3^h(\Delta L; O)$), and from there secondly to ($L_{30} + \Delta L$; $I_{3_{max}}/\sqrt{2} + \Delta I_3^h(\Delta L; O) - \Delta I_3^h(O; \Delta R)$) = ($L_{30} + \Delta L$; $I_{3_{max}}/\sqrt{2} + \Delta I_3^h(\Delta L; \Delta R)$)

Trying to understand the application to our measuring problem, we should have a look at Fig. 5 where the resonance curve of circuit III is represented as a function of the inductance L_3. If we tune C_3 to C_{30}, the resonance maximum will occur at $I_3 = I_{3_{max}}$ and $L_3 = L_{30}$ (L_0 in the figure) which is the inductance of circuit III without sample. If, on the other hand, C_3 is tuned to C_3^l or to C_3^h, the maximum of the I_3—L_3-curve is shifted to higher or to lower L_3-values, respectively, as is shown in Fig. 5 which illustrated that in these cases the 'working point' of circuit III lies on the lower or on the upper flank of the I_3-L_3-curve, respectively.

Our measuring procedure therefore has to run as follows: once we have to tune circuit III to $C_3 = C_3^h$ and circuit II to resonance and — keeping

$I_{3_{max}}/(2)^{1/2}$ automatically constant — to measure I_2 as a function of the sample-induced losses and susceptibility changes, and then we have to repeat this same measurement on the opposite flank of the resonance curve, i.e. in the case of $C_3 = C_3^l$ and $I_{30} = I_{3_{max}}/(2)^{1/2} = \text{const}$. Using Eqs. (9), (10) and (17), we can completely describe that procedure by a set of four equations:

$$R_{30} + \omega \cdot \Delta L_3 = \omega \cdot L_{23} \cdot ((I_{20} + \Delta I_2^h)/I_{30}) \cdot \sin \varphi^h \tag{18a}$$

$$R_{30} + \Delta R_3 = \omega \cdot L_{23} \cdot ((I_{20} + \Delta I_2^h)/I_{30}) \cdot \cos \varphi^h, \tag{18b}$$

where $I_{30} = I_{3_{max}}/(2)^{1/2}$ and $C_3 = C_3^h$, and additionally by

$$-R_{30} + \omega \cdot \Delta L_3 = \omega \cdot L_{23} \cdot ((I_{20} + \Delta I_2^l)/I_{30}) \cdot \sin \varphi^l \tag{19a}$$

$$R_{30} + \Delta R_3 = \omega \cdot L_{23} \cdot ((I_{20} + \Delta I_2^l)/I_{30}) \cdot \cos \varphi^l, \tag{19b}$$

if $C_3 = C_3^l$.

It is only elementary mathematics now to show that elimination of $\sin \varphi^h$ and $\cos \varphi^h$, and of $\sin \varphi^l$ and $\cos \varphi^l$, respectively, followed by neglect of second order terms, finally yields the result:

$$\omega \cdot \Delta L_3/R_{30} = \Delta I_2^h/I_{20} - \Delta I_2^l/I_{20} \tag{20}$$

$$\Delta R_3/R_{30} = \Delta I_2^h/I_{20} + \Delta I_2^l/I_{20}. \tag{21}$$

2. Measurement of I_3 during Automatic Regulation of $I_{2_{max}} = \text{const}$.

In this case we first tune circuits I and II to resonance and then circuit III additionally once to a C_3^h which, defining a suitable working point on the high-capacity resonance flank, is given by $I_{30} = I_{3_{max}} \cdot (2/3)^{1/2}$, and then to a C_3^l which also has to yield $I_{30} = I_{3_{max}} \cdot (2/3)^{1/2}$, and which thus defines the corresponding working point on the low capacity flank of the resonance curve. On both flanks ΔI_3 has to be measured as a function of the sample-induced high-frequency losses and susceptibility changes, while $I_{2_{max}}$ at the same time should be kept constant automatically.

Proceeding in this way the evaluation can be carried out as follows: elimination of $\sin \varphi$ and of $\cos \varphi$ from Eqs. (9) and (10) leads to

$$(R_{30} + \Delta R_3)^2 + (\omega \cdot (L_{30} + \Delta L_3) - 1/\omega \cdot C_3)^2 = \omega^2 \cdot L_{23} \cdot (I_2/I_3)^2, \tag{22}$$

i.e. to a function of type

$$I_3 = I_3(R_{30} + \Delta R_3,\ L_{30} + \Delta L_3). \tag{22a}$$

The intention of the next steps is to determine the points of inflection of that resonance function (22a) in order to expand it there into series of ΔR_3 and ΔL_3, hoping to get sufficiently good linear approximations of the by Eqs. (15) and (16), respectively. At first it can be type characterized concluded from the conditions

$$\partial I_3/\partial L_3 = 0 \tag{23}$$

and

$$\partial^2 I_3/\partial L_3^2 = 0 \tag{24}$$

that the points of inflection of the resonance curve are again determined by a certain C_3^h and by a corresponding C_3^l. The latter can be calculated from

$$-R_{30} = (2)^{1/2} \cdot (\omega \cdot L_{30} - 1/\omega \cdot C_3^l), \tag{25}$$

while the former follows from

$$R_{30} = (2)^{1/2} \cdot (\omega \cdot L_{30} - 1/\omega \cdot C_3^h). \tag{26}$$

In other words: C_3^h and C_3^l are just those capacity values which lead to I_3-values of magnitude $(2/3)^{1/2} \cdot I_{3_{max}}$.

Now we have to expand the functions

$$I_3^h = \omega \cdot L_{23} \cdot I_{20}/((R_{30} + \Delta R_3)^2 + (\omega \cdot (L_{30} + \Delta L_3) - 1/\omega \cdot C_3^h)^2)^{1/2} \tag{27}$$

and

$$I_3^l = \omega \cdot L_{23} \cdot I_{20}/((R_{30} + \Delta R_3)^2 + (1/\omega \cdot C_3^l - \omega \cdot (L_{30} + \Delta L_3)^2)^{1/2} \tag{28}$$

into series for $\Delta R_3/R_{30}$, $\Delta L_3/L_{30}$, and obtain to first order

$$-(\Delta R_3/R_{30}) = ((\Delta I_3^h/I_{30}) + (\Delta I_3^l/I_{30})) \cdot 3/4 \tag{29}$$

and

$$(\omega \cdot \Delta L_3/R_{30}) = ((\Delta I_3^l/I_{30}) - (\Delta I_3^h/I_{30})) \cdot (2)^{1/2} \cdot 3/4. \tag{30}$$

3. Simultaneous Recording of $I_{2_{max}}$ and I_3 during Automatic Regulation of $I_{1_{max}}$ = const.

Here circuit I plays the role of an extremely constant high-frequency generator, only while $I_{2_{max}}$ of circuit II as well as I_3, taken on one of the resonance flanks of circuit III, both will change markedly if a sample is put into the measuring coil, or if the sample's susceptibility or its losses start to change as a function of varying external parameters as temperature, magnetic field or applied pressure. Simultaneous measurement of $I_{2_{max}}$ and I_3

should therefore yield two independent informations during one run, and consequently expressions of type (15) and (16) should be evaluable at least approximatively.

In fact can they be deduced from Eqs. (9) to (12), using the following technique:

1. elimination of $\sin\psi$ and $\cos\psi$ from Eqs. (11) and (12) yields an expression which, together with Eq. (9), then enables the elimination of $\cos\varphi$ too;

2. substitution of I_2 and I_3 by $(I_{20}+\Delta I_2)$ and $(I_{30}+\Delta I_3)$, respectively, and expansion into a power series with respect to ΔI_2 and ΔI_3 finally yields the first result

$$\Delta R_3 = R_2\cdot(I_{20}/I_{30})\cdot(\Delta I_2/I_{30}) - (R_2\cdot(I_{20}/I_{30})^2 - \\ - ((\omega\cdot L_{12})^2/R_2)\cdot(I_{10}/I_{30})^2)\cdot(\Delta I_3/I_{30}); \tag{31}$$

3. rather analogously an equivalent expression can be found for $\omega\cdot\Delta L_3$ by elimination of $\sin\varphi$ and $\cos\varphi$ from Eqs. (9) and (10), neglect of second order terms, expansion into power series with respect to ΔI_2 nad ΔI_3, and by substitution of ΔR_3 by Eq. (31):

$$\omega\cdot\Delta L_3 = (\Delta I_2/I_{30})\cdot(I_{20}/I_{30})\cdot((\omega\cdot L_{23})^2 - 2.R_2\cdot R_{30})/ \\ /\omega\cdot(L_3 - 1/\omega^2\cdot C_3) - (\Delta I_3/I_{30})\cdot((\omega\cdot L_{23})^2\cdot(I_{20}/I_{30})^2 + \\ + 2\cdot R_{30}\cdot(R_2\cdot(I_{20}/I_{30})^2 - (I_{10}/I_{30})^2\cdot(\omega\cdot L_{12})^2/R_2))/ \\ /\omega\cdot(L_3 - 1/\omega^2\cdot C_3). \tag{32}$$

Among all the quantities occurring in Eqs. (31) and (32), the following ones are immediately measurable: I_{10}, I_{20}, I_{30}, ΔI_2, ΔI_3, ω, C_3. The total inductance L_3 of circuit III (in the case of empty measuring coil) is given by the resonance condition $L_3 = 1/\omega^2\cdot C_{30}$. The total dc-resistance R_{30} of circuit III can also be evaluated by the subsequently discussed calibration procedure. All other quantities on the right hand sides are sample-independent constants of the apparatus and could principally be measured by use of special calibration techniques. Although probably not very exact, it might be possible therefore to determine ΔR_3 and $\omega\cdot\Delta L_3$ even absolutely. We confine ourselves however to relative measurements, making use only of the linear relationships:

$$\Delta R_3 = A_1\cdot(\Delta I_2/I_{30}) - B_1\cdot(\Delta I_3/I_{30}) \tag{33}$$

$$\omega\cdot\Delta L_3 = A_2\cdot(\Delta I_2/I_{30}) - B_2\cdot(\Delta I_3/I_{30}), \tag{34}$$

and calibrating the factors A_1, A_2, B_1, B_2, by measurements on well known standard samples.

III. Calibration Procedure

What we are really measuring with the modified Fraunberger High-Frequency Apparatus are dc-output voltages $U_{2,m}$, $U_{3,m}$, given by the differential amplifiers of the respective measuring devices. These dc-voltages however are functions of the corresponding ac-voltages $U_{2,\,ind.}$ and $U_{3,\,ind.}$, originating in the coupling coils of the measuring devices (see Fig. 2) and depending therefore inductively on the high-frequency currents I_2 and I_3 of the oscillating circuits II and III, respectively. What we need are relations of type

$$I_2 = a_2 + b_2 \cdot U_{2,m} \tag{35}$$

$$I_3 = a_3 + b_3 \cdot U_{3,m} \tag{36}$$

in order to be introduced into the theoretical results of the above section, i.e. into the pairs of Eqs. (20)—(21), (29)—(30), and (33)—(34), respectively.

To succeed we suppose $U_{2,\,ind.}$ and $U_{3,\,ind.}$ to be always higher than the critical voltages U_{2c} and U_{3c} above which the diode characteristics of the measuring devices are linear. The diode currents I_{2d} and I_{3d} are then linear functions of $U_{2,\,ind.}$ and $U_{3,\,ind.}$, i.e.:

$$I_{2d} = \alpha_2 \cdot (U_{2,\,ind.} - U_{2c}) \tag{37}$$

$$I_{3d} = \alpha_3 \cdot (U_{3,\,ind.} - U_{3c}). \tag{38}$$

As $U_{2,m}$ and $U_{3,m}$ additionally are proportional to I_{2d} and I_{3d}, respectively, we find also

$$U_{2,m} = \gamma_2 \cdot (U_{2,\,ind.} - U_{2c}) \tag{39}$$

$$U_{3,m} = \gamma_3 \cdot (U_{3,\,ind.} - U_{3c}), \tag{40}$$

where

$$\gamma_2 = \alpha_2 \cdot \beta_2,\ \gamma_3 = \alpha_3 \cdot \beta_3 \tag{41}$$

and

$$U_{2,m} = \beta_2 \cdot I_{2d},\ U_{3,m} = \beta_3 \cdot I_{3d}. \tag{42}$$

Finally it follows from the coupling conditions

$$U_{2,\,ind.} = \omega \cdot L_{2c} \cdot I_2 \tag{43}$$

$$U_{3,\,ind.} = \omega \cdot L_{3c} \cdot I_3 \tag{44}$$

that

$$I_2 = (U_{2,m} + \gamma_2 \cdot U_{2c})/\gamma_2 \cdot \omega \cdot L_{2c} \tag{45}$$

$$I_3 = (U_{3,m} + \gamma_3 \cdot U_{3c})/\gamma_3 \cdot \omega \cdot L_{3c}, \tag{46}$$

and

$$\Delta I_2 = \Delta U_{2,m}/\gamma_2 \cdot \omega \cdot L_{2c} \tag{47}$$

$$\Delta I_3 = \Delta U_{3,m}/\gamma_3 \cdot \omega \cdot L_{3c}. \tag{48}$$

According to Eqs. (20), (21), (29), and (30), it is sufficient to know the ratios $\Delta I_2/I_2$ and $\Delta I_3/I_3$ in order to deduce from them the wanted normalized quantities $\Delta R_3/R_{30}$ and $\omega \cdot \Delta L_3/R_{30}$. Because of Eqs. (45)—(48) it is clear therefore that the aim of the following considerations should be to determine R_{30} and the products $\gamma_2 \cdot U_{2c}$, and $\gamma_3 \cdot U_{3c}$ by means of suitable calibration procedures. Let us therefore start from the proportionality

$$U_{3,\text{ind.}} = a_3 \cdot \omega \cdot L_{23} \cdot I_2/(R_{30}^2 + (\omega \cdot L_3 - 1/\omega \cdot C_3)^2)^{1/2}, \tag{49}$$

where a_3 means a certain proportional factor. Then we have

$$U_{2,m} = \gamma_2 \cdot (L_{2c} \cdot \omega \cdot I_2 - U_{2c}) \tag{50}$$

and

$$U_{3,m} = \gamma_3 \cdot (a_3 \cdot \omega \cdot L_{23} \cdot I_2/(R_{30}^2 + (\omega \cdot L_3 - 1/\omega \cdot C_3)^2)^{1/2} - U_{3c}). \tag{51}$$

Elimination of I_2 yields

$$\frac{(U_{2,m} + \gamma_2 \cdot U_{2c})^2}{\gamma_2^2 \cdot R_{30} \cdot A} - \frac{(\omega \cdot L_3 - 1/\omega \cdot C_3)^2}{R_{30}^2} = 1, \tag{52}$$

with

$$A = (U_{3,m} + \gamma_3 \cdot U_{3c})^2 \cdot (\omega \cdot L_{2c}/\gamma_3 \cdot a_3 \cdot \omega \cdot L_{23})^2. \tag{53}$$

If A is kept constant, Eq. (52) obviously is a hyperbolic relation between $U_{2,m}$ and $1/\omega \cdot C_3$. Thus we deduce the following method of calibration:

1. Adjust circuits I, II and III as described in § 3, section II, point 1, and regulate I_3 then automatically constant.

2. Measure $U_{2,m}$ as a function of C_3 and draw the respective branch of the hyperbola.

3. Choose three arbitrary points of the hyperbola and substitute their coordinates as well as those of the angular point into Eq. (52), thus getting four equations for the four unknown quantities $\gamma_2 \cdot U_{2c}$, $\omega \cdot L_3$, R_{30}^2 and $\gamma_2^2 \cdot R_{30} \cdot A$, which then can be evaluated.

4. Repeat the procedure described in points 1) to 3), but adjust circuit III to another value $U_{3,m}$ as at the first time; so you will get a second set of values $\gamma_2 \cdot U_{2c}$, $\omega \cdot L_3$, R_{30}^2 and $\gamma_2^2 \cdot R_{30} \cdot A$, which on the one hand will illustrate the accuracy of absolute measurement, while it on the other hand will enable you to determine $\gamma_3 \cdot U_{3c}$ too, which, according to Eq. (53), depends linearly on $U_{3,m}$ and on $(\gamma_2^2 \cdot R_{30} \cdot A)^{1/2}$:

$$(\gamma_2^2 \cdot R_{30} \cdot A)^{1/2} = \text{const.} \cdot (U_{3,m} + \gamma_3 \cdot U_{3d}),$$

with

$$\text{const.} = \omega \cdot L_{2c}/\gamma_3 \cdot a_3 \cdot \omega \cdot L_{23}.$$

§ 4. Examplification of Sensitivity and Applicability

One of the crucial tests of the modified Fraunberger apparatus doubtlessly can be carried out measuring the susceptibility of paramagnetic salts. Let us therefore start with:

1. Calibration Measurements Using Paramagnetic $MnSO_4 \cdot H_2O$

The calibration procedure described under § 3, point III, yielded the following constants of our apparatus:

$$\overline{\gamma_2 \cdot U_{2d}} = 173.5 \text{ mV} \pm 7\% \tag{54a}$$

$$\overline{\gamma_3 \cdot U_{3d}} = 168 \text{ mV} \pm 7\% \tag{54b}$$

$$R_{30} = 9.55\ \Omega \pm 6\% \tag{54c}$$

$$\omega \cdot L_3 = 561.5\ \Omega \pm 1.5\%. \tag{54d}$$

Using these values and measuring 10.4985 grams of paramagnetic $MnSO_4 \cdot H_2O$-powder at room temperature due to method 2. (see § 3, point II), we got changes of inductance and of resistance amounting to

$$\omega \cdot \Delta L = 50.2 \cdot 10^{-3}\ \Omega$$

$$\Delta R = 7.74 \cdot 10^{-3}\ \Omega.$$

Substituting into Eqs. (7) and (8) and taking into account the geometric data of the measuring coil, i.e. $n = 3.5$, $F = 3.5^2 \cdot \pi$ cm^2, $l = 4.5$ cm, we found a susceptibility of

$$\chi = 5.8 \cdot 10^{-5} \text{ [(Gauß/Oe)/gram]}$$

and an imaginary part μ_i of the complex permeability of

$$\mu_i = 1.2 \cdot 10^{-4} \text{ (e. m. u./gram).}$$

According to Landolt-Börnstein's handbook (1966), the best χ-value of $MnSO_4 \cdot H_2O$-powder at room temperature is $8.4 \cdot 10^{-5}$ [(Gauß/Oe)/gram].

Thus we state a deviation of 30% down to lower susceptibility. The agreement within 30% appears to be satisfactory in view of the special geometry of the measuring coil and of the cylindrical powder-tube: while the diameter of the latter amounts to one inch (thus determining a sample height of about 3 cm in the case of 10.5 g $MnSO_4 \cdot H_2O$), the dimensions of the coil are 7 cm in diameter, 4.5 cm in length and 3.5 windings of a copper tube of 6 mm outside diameter and 4 mm inside diameter which is flown through by water of constant temperature. It is clear that under such conditions a coupling factor has to be taken into account which we therefore, renouncing on its theoretical estimation, postulate to compensate just the above mentioned difference of 30% between our χ-value and the exact result.

To give an impression of the sensitivity of our apparatus, let us supplement the signal/noise ratio (s/n) of the above calibration measurement. We were working at (s/n) $\approx$ 36 which is equivalent to a sensitivity S of

$$S_{max} = 2.3 \cdot 10^{-6} \text{ [(Gauß/Oe)/gram].}$$

As that noise however was of purely mechanical type, arising from a not very well working mounting system (which on the other hand was good enough for our purposes), it could be reduced by at least a factor ten. If additionally the total volume of the measuring coil would be used for measurement at sufficiently large samples, and if the coil would no longer be flown through by water (which causes an increase in damping by a factor 4 and is not necessary for room temperature measurements), a maximum sensitivity of

$$S_{max} = 1 \cdot 10^{-8} \text{ [(Gauß/Oe)/gram]}$$

should really be possible. The corresponding sensitivity in measuring the high-frequency losses, particularly the Rayleigh constant α, then turns out to come to about

$$(S\alpha)_{max} = 7 \cdot 10^{-8} \text{ [(Gauß/Oe}^2\text{)/gram].}$$

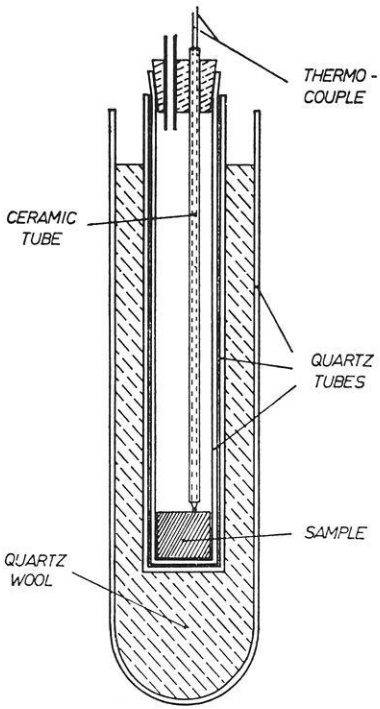

Fig. 6. Diamagnetic quartz vessel of low heat conductivity. The inner quartz tube (one inch in diameter) can be evacuated. The outside diameter amounts to 60 cm. After having been heated up to, say, 200 °C, the cooling process of the quartz vessel starts at a cooling rate of about 0.5 °C/min which however decreases with decreasing temperature

2. Temperature-Dependence of Susceptibility and Losses of a Standard Basalt Sample of the 'Rauher Kulm' (Bavaria)

This example gives us the opportunity to point out briefly how we solved the problems arising from the above estimated extremely high sensitivities if measurements are carried out at varying temperatures. The difficulty was to find materials having strictly temperature-independent susceptibilities and losses, and to avoid even the slightest changes in the dc-resistance of the measuring coil. It was therefore impossible to put the coil simply inside a usual furnace or a dewar vessel (in the case of low temperatures), and it was also completely impracticable to use an electrically heated furnace inside the measuring coil. Hence, there remained the only chance to build a totally diamagnetic quarz-vessel of relatively high heat capacity and low heat conductivity a sketch of which is shown in Fig. 6. For high-temperature measurements we heat that vessel — which contains the

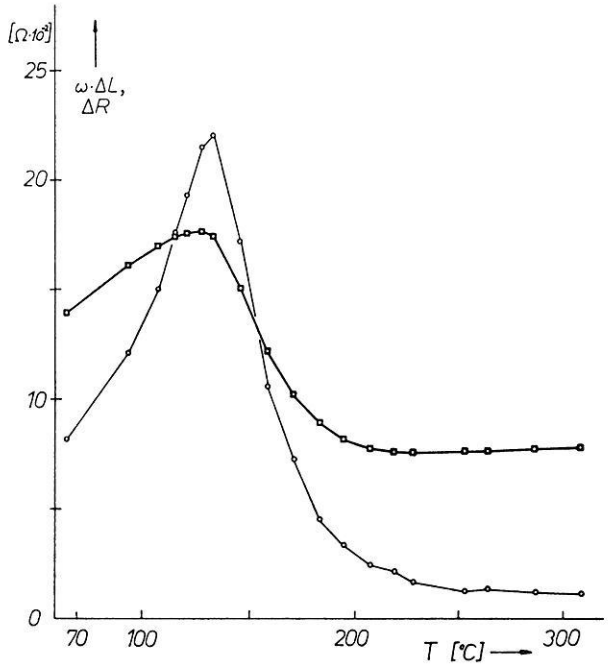

Fig. 7. Temperature dependence of susceptibility (—□—□—) and losses (—○—○—) of a standard basalt core (inch dimensions) of the 'Rauher Kulm' (Bavaria). Measurement was carried out during cooling down from 350 °C. The sample-containing inner quartz tube (see Fig. 6) was evacuated. The decrease of both susceptibility and losses is blurred over a temperature interval of about 80 °C. According to Bleil (1973), there holds a quadratic relationship between the Curie temperature T_c and the titanium concentration x of the titanomagnetite series of type $Fe_{3-x}Ti_xO_4$. He found best fit with his own measurements as well as with those of Akimodo, Katsuma and Yoshida (1957), Uyeda (1958) and Ozima and Larson (1970), when supposing: $T_c = 583.2 - 567.4 \cdot x - 185.5 \cdot x^2$ [°C]. Thus the titanium concentration of the investigated R. K.-sample is spread over an interval ranging from about $x = 0.55$ up to $x_{max} = 0.66$

sample in its inner evacuated tube — in a furnace located outside of the measuring coil, put it then into that coil which is water-cooled in the way described above, and measure during cooling down of the sample. Low-temperature measurements can be performed by pouring liquid nitrogen into the inner quartz tube and measuring then during warming up to room temperature.

To attend now to the announced result got by the just mentioned technique, let us have a look at Fig. 7 which shows the temperature dependence of both the susceptibility χ and the Rayleigh constant α of a standard basalt core (usual inch-dimensions, i. e. one inch in diameter and one inch in

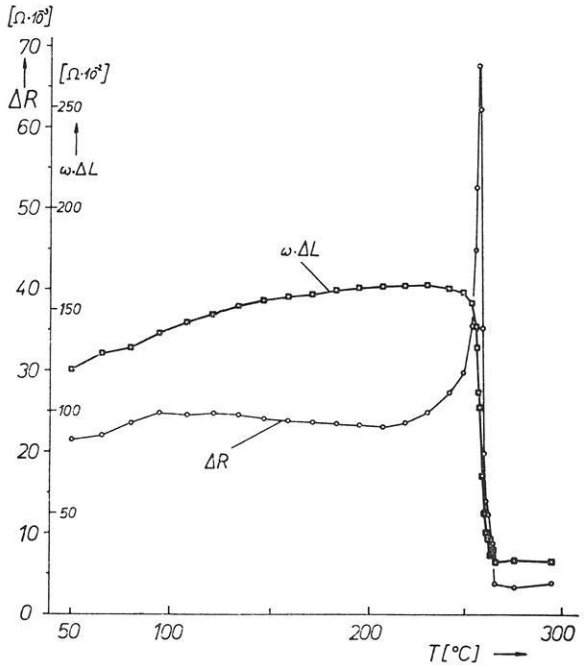

Fig. 8. Curie point of a yttrium iron garnet (YIG) single crystal. Susceptibility (—□—□—) and losses (—○—○—) have been measured during cooling down from about $1.5 \cdot T_c$ to room temperature. For more details see § 4., point 3. of the text

height) of the 'Rauher Kulm' (Bavaria). During heating and measuring the sample-containing inner quartz-tube was evacuated thus preventing even slight oxidation the non-occurrence of which could be proved by repeating the whole measurement which then gave exactly the previously measured curves. If there were only one definite Curie point, the high-temperature flanks of both curves should fall off much more rapidly, i.e. within less than 5 degrees centigrade (see the following example). It turns out therefore that the Curie temperatures are spread over an interval of about 80 degrees centigrade which indicates titanium concentrations of the titanomagnetite ore grains varying from about 55 mole percent Ulvöspinel up to at least 66 mole percent.

3. Further Examples of Curie Points

Fig. 8 shows the neighbourhood of the Curie point of a yttrium iron garnet-single crystal. There is a very sudden jump of the susceptibility and a correspondingly sharp maximum (infinity point) of the high-frequency losses. The small secondary peak of the susceptibility curve is due to the

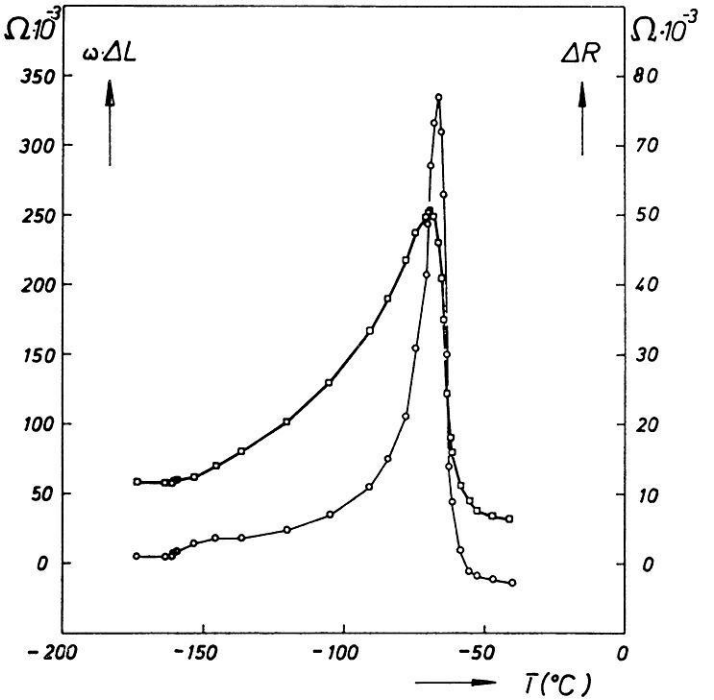

Fig. 9. Curie point of a synthetic $MgAlFeO_4$-spinel. The temperature dependence of the high-frequency susceptibility (—□—□—) and of the losses (—○—○—) has been measured during warming up to room temperature

superimposed earth-magnetic dc-field which, according to Markert (1971), causes parallel pumping resonances of the fluctuating spin systems governing the magnetic properties near the Curie point (A more detailed study of these effects will be published in phys. stat. sol. in the near future). To demonstrate also a low-temperature Curie point, Fig. 9 shows the susceptibility and the losses of a synthetic $MgAlFeO_4$-spinel.

4. Low-Temperature Phase Transition of Magnetite

There is a low-temperature phase transition point of pure magnetite where the crystal lattice changes from face-centred cubic to rhombohedral symmetry or vice versa, depending on whether the sample becomes cooled down or warmed up during measurement. Because of the occurrence of temperature hysteresis the transition temperature can vary in between at least —150 °C and —140 °C. An usual method of detecting such transition points is X-ray analysis but it was expected that measurements of susceptibility and high-frequency losses also might indicate it. And in fact a rather

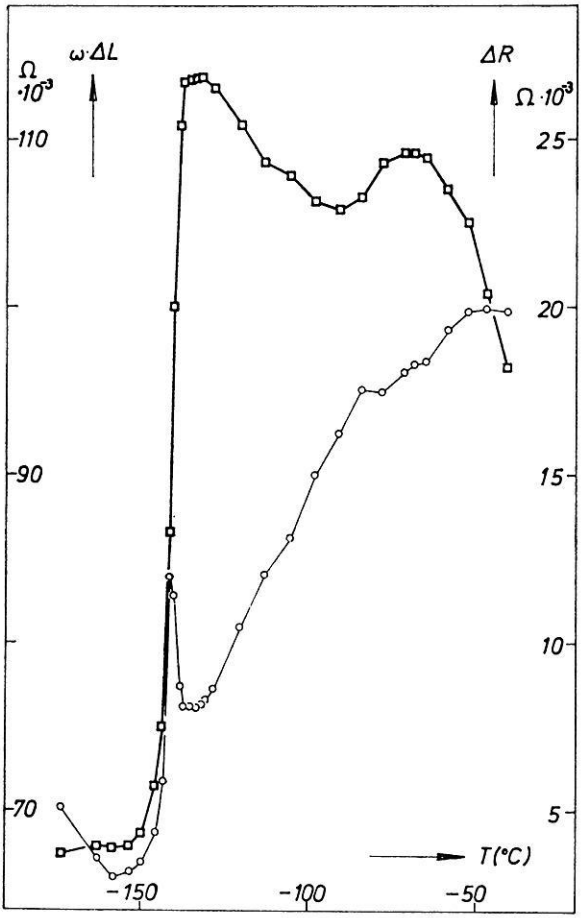

Fig. 10. Low-temperature phase transition point of pure synthetic magnetite. Within a temperature interval ranging from, say, −155 °C up to −130 °C, both curves run quite specularly to the corresponding ones shown in Fig. 8. Again the susceptibility curve is marked by '—□—□—', while the losses are characterized by '—○—○—'

strong effect could be observed as is shown in Fig. 10. Comparison with Fig. 8 verifies that in the neighbourhood of both of these phase transitions the susceptibilities as well as the high-frequency losses underlie exactly the same law, thus indicating phase transitions of the same type, i.e. of second order — which order, at least in the well analysed case of YIG, doubtlessly governs the magnetization break-down at the Curie point.

As it promised to be of certain geophysical interest, we repeated the above measurement using now a natural magnetite single crystal (from

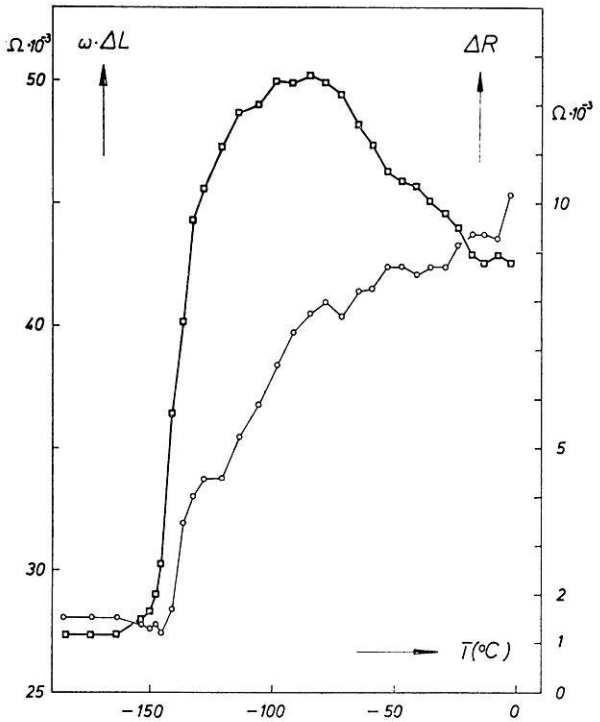

Fig. 11. Low-temperature phase transition point of a natural magnetite single crystal (from Zöptan/Sobolin, Czechoslovakia). The very sharp maximum of the high-frequency losses shown in Fig. 10., does not occur at all — probably because of the relatively high impurity content of such natural samples

Zöptan/Sobolin). The result is illustrated in Fig. 11. It is obvious from these curves that the magnetite-low temperature phase transition depends very sensitively on the — relatively high — impurity content always occurring in such natural crystals (A more detailed analysis of the influence of the titanium concentration on such phase transition points will be given elsewhere).

5. Influence of dc-Magnetic Fields on Susceptibility and Losses of a Standard Basalt Sample

Using large Helmholtz-coils in order to superimpose dc-magnetic fields up to 400 Oe in parallel to the ac-field, we studied also how the susceptibility and the high-frequency losses of a basalt standard sample of the 'Rauher Kulm' (Bavaria) vary with the dc-field intensity. Fig. 12 shows the result measured along the positive part of a minor hysteresis loop, i.e.

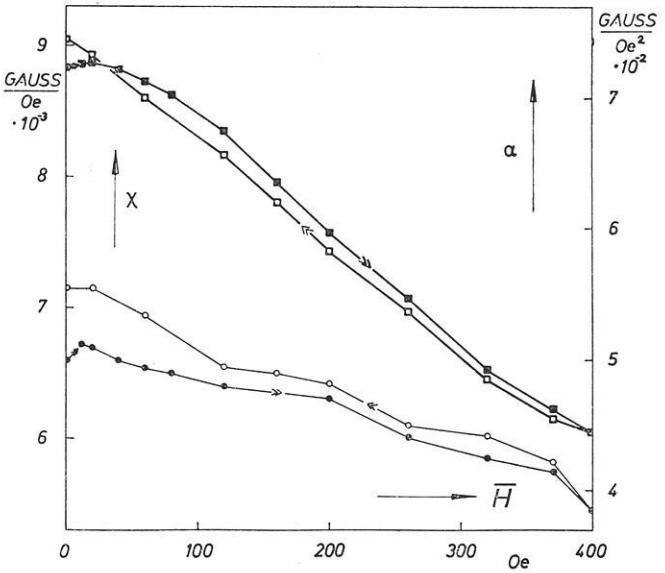

Fig. 12. Influence of dc-magnetic fields on susceptibility (—□—□—) and losses (—○—○—) of a standard basalt sample of the 'Rauher Kulm' (Bavaria). Measurement was carried out along the positive part of a minor hysteresis loop, i.e. had started from the point of minor negative remanence towards the minor reversal point (at 400 Oe), and had ended up at the minor positive remanence point. A first interpretation has been sketched roughly in § 4, point 5 of the text

from negative remanence to the minor reversal point (at 400 Oe) and back to the positive remanence point. As may be seen from the figure, particularly the curve of the losses — but also the susceptibility curve — does not come back to its origin at $\overline{H} = O$ as they should do however if the sample were in its so-called 'cyclic state', i.e. if each minor loop as a whole would be reproducable. What we suppose — and shall discuss elsewhere — is a state of mechanical non-equilibrium caused by means of irreversible deformation due to magnetostriction of the titanomagnetite ore grains relative to their rather inelastic silicate matrix.

6. Anisotropy of Susceptibility and Losses of a Basalt Sample from Mt. Etna

Intending to measure rather small anisotropies, we first proved that the apparatus really was well-working with regard to this kind of application. Therefore a polycrystalline rod of magnetite from Kirunavaara (North of Sweden) was rotated around its short axis — oriented perpendicularly to the axis of the oscillating coil —, while the measuring signals (induced on one flank of the resonance curve and after readjusting also on the other) were recorded versus time. The result, the shape anisotropy of

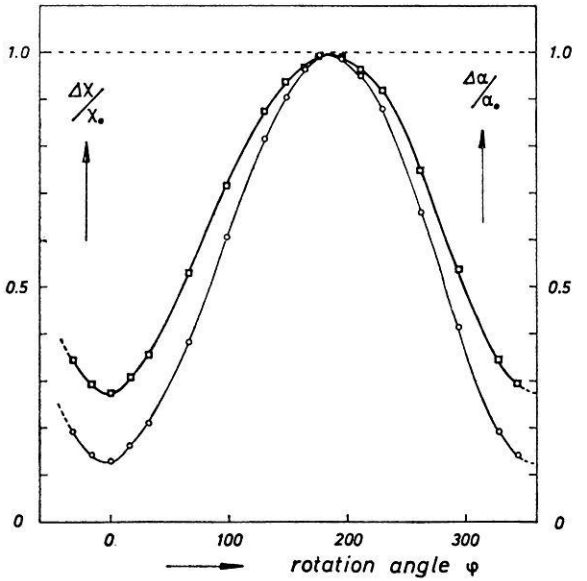

Fig. 13. Shape anisotropy of a polycrystalline rod of magnetite (from Kirunavaara, North of Sweden) the short axis of rotation of which was oriented perpendicularly to the axis of the oscillating coil. The demagnetizing factor amounted to 0.26 [Oe/Gauß]. The susceptibility (—□—□—) and the losses (—○—○—) are plotted as percentage deviation from the respective maximum values χ_0 and α_0 (with α_0 meaning Rayleigh's constant). Obviously the losses show stronger anisotropy than the susceptibility

susceptibility and losses, is shown in Fig. 13; according to a demagnetizing factor of 0.26 (Oe/Gauß), a strong effect had to be expected and took place indeed.

These magnitudes decreased significantly when we attended to anisotropy measurements to be carried out on a basalt core of usual inch-dimensions, originating from a lava flow of Mt. Etna (gathered near Fornazzo). The curves which we now got are illustrated in Fig. 14. The maximum susceptibility change amounts to $80 \cdot 10^{-6}$ (Gauß/Oe), the loss amplitude comes to $60 \cdot 10^{-5}$ (Gauß/Oe^2). This example characterizes the sensitivity of those anisotropy measurements we can perform at the moment using samples of standard inch dimensions and our standard measuring coil described above: the minimum susceptibility amplitude therefore comes to about $10 \cdot 10^{-6}$ (Gauß/Oe), while the loss amplitude should not fall below $8 \cdot 10^{-5}$ (Gauß/Oe^2). If we however would work with a specially proportioned and very well mounted coil, at least another factor ten could be won — a factor 4 for instance simply can be obtained by omitting water cooling of the oscillating coil.

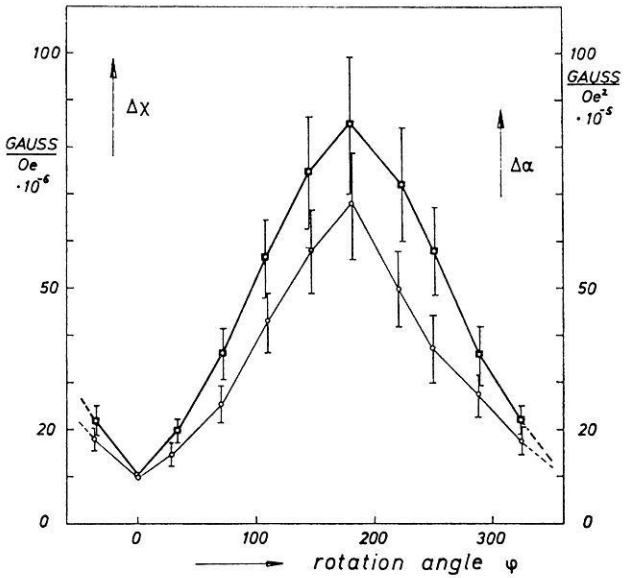

Fig. 14. Anisotropy of susceptibility (—□—□—) and losses (—○—○—) of a basalt sample (standard inch dimensions) from Mt. Etna. The error intervals are depending on the rotation angle ψ because of the fact that we plotted only the changes $\Delta\chi$ and $\Delta\alpha$ versus ψ — and not, for instance, the normalized quantities $\Delta\chi/\chi$ and $\Delta\alpha/\alpha$ the error of which would not decrease to zero at $\psi = O$

On the other hand our present device enables us to do anisotropy measurements also at temperatures varying from nitrogen boiling point up to about 400 °C and this might open another field of interesting applications.

Acknowledgements. We are very indebted to Prof. Dr. F. Fraunberger (Phys. Institut, Gesamthochschule Bamberg) who introduced us to his high-frequency method, and who also supported the present investigations financially as well as by contributing some of the experimental equipment.

There were many persons advising and helping us in performing the experimental and theoretical details. Particularly we wish to thank Prof. Dr. G. Angenheister (head of the 'Institut für Angewandte Geophysik', Univers. of Munich), Dr. N. Petersen, Dr. E. Schmidbauer, Prof. Dr. H. Soffel, Dipl. Phys. U. Bleil (all from 'Institut für Angewandte Geophysik', Univers. of Munich), as well as Prof. Dr. K. Stierstadt and Dr. H.-J. Bauer (both from 'Sektion Physik', Univers. of Munich).

Moreover this work was supported by the Deutsche Forschungsgemeinschaft.

References

Akimoto, S., Katsuma, T., Yoshida, M.: Magnetic properties of the Fe_2TiO_4—Fe_3O_4 system and their change with oxidation. J. Geomag. Geoelect. *9*, 165—178, 1957

Bleil, U.: Private communication 1973
Ehrenfest, P.: Proc. Acad. Sci. Amsterdam *36*, 153, 1933
Fraunberger, F.: Über eine Hochfrequenzmethode für metallkundliche Untersuchungen an magnetischen Legierungen. Z. Metallk. *46*, 749–751, 1955
Feldtkeller, R.: Spulen und Übertrager. 2nd edition, Vol. I: Spulen. Stuttgart: S. Hirzel 1949
Fuller, M. D.: The A. C. bridge method. In: Methods in palaeomagnetism. Eds. Collinson, D. W., Creer, K. M., Runcorn, S. K., Amsterdam–London–New York: Elsevier Publishing Comp. 1967
Kneller, E.: Ferromagnetismus. Berlin–Göttingen–Heidelberg: Springer 1962
Landolt-Börnstein: Handbook on: Magnetische Eigenschaften der Koordinations- und Metallorganischen Verbindungen der Übergangselemente. By Hellwege, K.-H., Hellwege, A. M., eds., Berlin–Heidelberg–New York: Springer 1966, New Series II/2, p. 2–68
Markert, H.: Interpretation of the Hopkinson secondary maximum in terms of parallel pumping theory. Z. f. Naturf. *26a*, 1764–1766, 1971
Ozima, M., Larson, E. E.: Low- and high-temperature oxidation of titanomagnetite in relation to irreversible changes in the magnetic properties of submarine basalts. J. Geophys. Res. *75*, 1003–1017, 1970
Petersen, N.: A High-frequency method for the measurement of curie temperatures of ferrimagnetic minerals. In: Methods in palaeomagnetism. by Collinson, D. W., Creer, K. M., Runcorn, S. K., eds. Amsterdam–London–New York: Elsevier Publishing Comp. 1967
Schwarz, O.: Diplomarbeit, Sektion Physik, Univers. of Munich 1963
Uyeda, S.: Thermo-remanent magnetism as a medium of palaeomagnetism, with special reference to reverse thermo-remanent magnetization. Jap. J. Geophys. *II*, 1–123, 1958

Dr. H. Markert
Universität Bayreuth
D-8580 Bayreuth
Münzgasse 9
Federal Republic of Germany

K.-H. Trissl
G. J. Zimmermann
Sektion Physik
University of Munich
D-8000 München
Federal Republic of Germany

Note Added in Proof. In Figs. 13 and 14 the scale numbers of the rotation angle φ have to be divided by 2.